Published in final edited form as:
Neuroimage. 2012 November 1; 63(2): 947–958. doi:10.1016/j.neuroimage.2012.03.092.

Mapping directionality specific volume changes using tensor based morphometry: An application to the study of gyrogenesis and lateralization of the human fetal brain

Vidya Rajagopalan[a,*], **Julia Scott**[a], **Piotr A. Habas**[a], **Kio Kim**[a], **Francois Rousseau**[b], **Orit A. Glenn**[c], **A. James Barkovich**[c], and **Colin Studholme**[a]

[a]Biomedical Image Computing Group, Departments of Pediatrics, Bioengineering, and Radiology, University of Washington, Seattle, WA 98195, USA

[b]Image Sciences, Computer Sciences and Remote Sensing Laboratory, Unité Mixte de Recherche 7005, Centre National de la Recherche Scientifique-University of Strasbourg, 67412 Illkirch, France

[c]Department of Radiology and Biomedical Imaging, University of California San Francisco, San Francisco, CA 94131, USA

Abstract

Tensor based morphometry (TBM) is a powerful approach to analyze local structural changes in brain anatomy. However, conventional scalar TBM methods do not completely capture all direction specific volume changes required to model complex changes such as those during brain growth. In this paper, we describe novel TBM descriptors for studying direction-specific changes in a subject population which can be used in conjunction with scalar TBM to analyze local patterns in directionality of volume change during brain development. We also extend the methodology to provide a new approach to mapping directional asymmetry in deformation tensors associated with the emergence of structural asymmetry in the developing brain. We illustrate the use of these methods by studying developmental patterns in the human fetal brain, *in vivo*. Results show that fetal brain development exhibits a distinct spatial pattern of anisotropic growth. The most significant changes in the directionality of growth occurs in the cortical plate at major sulci. Our analysis also detected directional growth asymmetry in the peri-sylvian region and the medial frontal lobe of the fetal brain.

Keywords

Structural MRI; Fetal imaging; tensor based morphometry; directional growth modeling; brain development

* Biomedical Image Computing Group, Departments of Pediatrics, Bioengineering, and Radiology, University of Washington, Seattle, WA 98195, USA, Tel.: (+ 1) 206 221 2993 vidyaraj@uw.edu (Vidya Rajagopalan).

1. Introduction

Tensor based morphometry (TBM) is now widely used as a method to detect structural brain differences across a population or across time. TBM studies involve statistical analysis of deformation fields computed from non-rigid registration of different anatomies. Scalar TBM, in its original form [7], continues to be used to analyze structural changes caused by neurodegenerative conditions in adult brains [44] [40].

More recently, TBM is also being used for modeling of growth in developing brains [26] [24] [11] [2] [43] [38]. Formation of a sulcated adult brain from a smooth fetal brain is characterized by simultaneous increases in tissue volume and complexity of cortical shape. This suggests that the brain maturation manifests as an age-related series of directionally specific volume expansions with locally varying growth rates. In order to fully understand the development of brain morphology, we need to study both the magnitude and direction of local tissue volume increase.

However, a key limitation of scalar TBM is that it explicitly ignores directionality of volume changes. The multivariate, strain tensor metric proposed by Lepore et al. [27], analyzes the entire deformation gradient tensor. This metric ignores volume independent, local orientation changes within the brain, and is unable to specify the directionality of shape change for intuitive anatomical understanding [48]. Studying the complex shape changes during brain development is a key motivation for the extension of TBM to look at patterns of direction specific volume change. For example, the Sylvian fissure in the fetal brain is related to superior-inferior expansions in the frontal and temporal lobes along with left-right contractions in the inferior aspect of the frontal cortex and superior aspect of the temporal cortex, which has been described as a sharpening angle between the insula and the adjacent gyrus [32].

Directional growth information is particularly helpful in modeling fetal, human brain development. During gestation, the smooth fetal brain undergoes a series of interconnected increases in regional tissue volume in tissue volume and shape to form a complex, sulcated adult brain [36] [17] [35] [16]. Historically, fetal brain growth studies have been based on global tissue volume or gyrification indices [5] [3]. More recently, fetal brain growth is modeled using scalar morphometric models that characterize primary gyro-genesis as a deepening of the sulcus through curvature [9, 16] or depth [18] measurements on a surface representation. These models do not describe the full spatial pattern of cortical folding because they do not assess cortex and underlying tissue simultaneously and in that way are limited in how they model the folding process. However, global analysis of volume and gyrification show that cortical gyrification occurs in conjunction with tissue volume increase in the fetal brain[22].

In this paper, we build on our previous work [33] on studying direction specific volume changes associated with brain deformation. We use the mathematical foundations of the metrics presented in [33] and extend it to quantify directional patterns of volume change across a population. We present a test to detect principal growth directions at a particular tissue location. Using the principal growth direction as a baseline, we propose statistical metrics to localize regions showing significant changes in directionally specific growth. In the current paper, we have also enhanced the proposed metrics to be able to detect asymmetric deformation corresponding to the emergence of structural asymmetry in the developing brain.

We use the proposed metrics to model the primary patterns of directionally specific growth associated with fetal brain development. We also characterize significant increase/decrease in growth rate along these directions. By studying brain development as a combination of

volume and direction change patterns, we are able to better characterize the mechanism of brain growth than the study of scalar volumes changes alone. By including directional information in the study of tissue volume change, we have for the first time identified specific directional changes in local brain size that result in local volume changes. We then demonstrate the correlation between local volume change and gyrification by modeling brain growth as a series of directionally specific local changes in brain size. By using the proposed metrics in a group comparison framework, we detect directional asymmetry in growth patterns underlying the emergence of interhemispheric asymmetries in early fetal development. While hemispheric asymmetry has been detected in other scalar TBM models [4, 23], we uniquely showed interhemispheric differences in local brain size along specific directions by using a consistent co-ordinate system. The study extends the timeline of brain developmental trajectories into the fetal period and enhances our understanding of the early brain development.

2. Methods

A cross-sectional population of N subjects, are spatially normalized such that each subject anatomy is aligned to common, anatomical coordinate system, also known as average space. For each subject, we compute a transformation T_i, where $i = 1, 2, \ldots N$, which maps the anatomical changes required to spatially normalize that particular subject to the average space. At each voxel p, the local change can be derived from the Jacobian matrix which is defined as the spatial gradient of the transformation vector $T_i^p = [T_{i,x}^p, T_{i,y}^p, T_{i,z}^p]$

$$J_i^p = \begin{bmatrix} \frac{\partial T_{i,x}^p}{\partial x} & \frac{\partial T_{i,x}^p}{\partial y} & \frac{\partial T_{i,x}^p}{\partial z} \\ \frac{\partial T_{i,y}^p}{\partial x} & \frac{\partial T_{i,y}^p}{\partial y} & \frac{\partial T_{i,y}^p}{\partial z} \\ \frac{\partial T_{i,z}^p}{\partial x} & \frac{\partial T_{i,z}^p}{\partial y} & \frac{\partial T_{i,z}^p}{\partial z} \end{bmatrix}. \quad (1)$$

By computing J at each voxel, we form a map of local changes across the subject population. In this paper, we use information from the tensor decomposition properties of the Jacobian matrices to extract deformation direction.

2.1. Deformation Direction Vector (DDV)

The principal deformation direction can be obtained from the principal component of the Jacobian matrix at each voxel. In order to avoid stability issues associated with eigen analysis of any Jacobian matrix, we leverage the polar decomposition property of J [12] to compute the primary deformation direction indirectly. At each voxel, the Jacobian matrix, being a second order tensor, can be separated into a rotational and a strain component [31].

$$J = RS = S'R \quad (2)$$

where R is the orthogonal, rotation tensor such that $R^{-1} = R^T$ and $\det(R) = +1$. S and S' are symmetric, positive definite tensors known as the right and left stretch tensors respectively. S and S' are related by $S' = RSR^T$. The stretch tensors can be computed from the following relationship

$$S = J^T J = \sqrt{C} \quad S' = JJ^T = \sqrt{C'}$$

C and C' are known as the right and left Cauchy-Green tensors (CGT), respectively.

As illustrated Figure 1, this decomposition is analogous to first stretching the voxel by S and then rotating it by R to realize the deformation [8]. Therefore, the direction of deformation, is computed by extracting the principal eigenvector of strain (**e**) from S, and rotating this by R yields the DDV. Here, we would like to emphasize that **e** only specifies the principal direction of strain and not the direction of the complete deformation. For each subject, we compute a DDV map (DDV at each voxel), which is used to analyze local changes in directionality.

Statistical Analysis DDV—The DDV map can then be used in the TBM framework to detect population wide changes. In Equation 3, the basis vectors correspond to the three primary, orthogonal directions in reference anatomy: inferior-superior, left-right and anterior-posterior. The scalar multiplicative factors (x,y,z) from the DDV are separated to form three directional component maps (DCM). The DCM can be considered statistically independent within the single deformation tensor, as knowledge of the scalar component along one direction gives no information about the other two values in the DDV.

$$DDV(x_i, y_i, z_i) = x_i(1,0,0) + y_i(0,1,0) + z_i(0,0,1) \quad (3)$$

In order to minimize local variations in direction arising as a result of residual mismatch after registration, the DCMs are individually smoothed. Although conventional TBM studies apply smoothing to the deformation maps directly, smoothing the DCMs in this application has the following advantages: it avoids the artificial spatial uniformity that is introduced in the maps and maximizes the sensitivity of our directional metric to small but relevant anisotropic changes in the anatomy. In this work, the size of the Gaussian smoothing kernel (σ= 2 mm) was chosen experimentally to maximize statistical power and minimize registration mismatch. Kernel sizes larger than 2 mm diminished the power of the statistical tests by averaging out meaningful local variations, while smaller kernel sizes did not sufficiently diminish the effect of registration mismatch.

Regression—Using regression, we examine if there is a relationship between the basis vectors and variables of interest related to each subject (such as age or clinical criteria) using the multivariate general linear model at each voxel [39]. Growth models of DDV with respect to age can be performed using multivariate, multiple regression as shown in Equation 4. Here A corresponds to the vector of DCM values at each voxel, $V_1,\ldots, V_m$ are the independent variables (age, gender, clinical condition, etc.) and ε are the errors. (The matrix dimensions of each of the variables are indicated below each variables in Equation 4). Linear least square methods are used to solve for $\beta_1,\ldots, \beta_m$ at each voxel.

$$\underset{(n\times 3)}{A} = \underset{(n\times 1)(1\times 3)}{V_1\beta_1} + \ldots + \underset{(n\times 1)}{V_m\beta_m} + \varepsilon \quad (4)$$

Hypothesis Testing—Resulting regression coefficient ($\beta_1,\ldots, \beta_m$) maps are tested for significance using a standard t-test. Statistical significance was computed and these were corrected for multiple comparisons using permutation tests [30]. The corrected p-value maps of the three directional components can then be analyzed individually or can be combined using Fisher's meta-analysis method [10] for independent tests. Let $h_o^1, h_o^2 \ldots h_o^k$ be the k independent null hypotheses being tested. Fisher's meta-analysis tests the null hypothesis that all the individual null hypotheses are true. The alternate hypothesis of the meta-analysis is that at least one of the individual null hypothesis is false. The p-values from the individual tests are combined using the formula $k = -2\sum_{i=1}^{k} \log_e(p_i)$ $\log_e(p_i)$ where pi is the p-value of

the i^{th} individual hypothesis test. The meta-analysis statistic κ has a chi-squared distribution under the null hypothesis with $2k$ degrees of freedom.

The $\beta_1,\ldots,\beta_m$ values are estimates of increase or decrease in volume along a particular direction and the hypothesis tests estimate statistical significance of these changes. Multivariate hypothesis tests are not well suited for this metric as a meaningful covariance between directions cannot be established.

2.2. Principal Growth Direction (PGD)

In scalar TBM, the definition of volume change is well understood, i.e. undeformed voxels have a Jacobian determinant of 1 and any deviation from this value is considered as change. For directional properties, such a distinct baseline does not exist. To establish a baseline, we make use of the DDV map for each subject which provides orientation information specific to each subject at any given location. As described in Equation 5, PGD at a voxel is defined as the DDV (of a single subject) which has the least circular distance [28] from DDVs of all the other (N–1) subjects.

$$PGD=\arg\min_{DDV_i}\left(\sum_{j=1}^{N}\frac{1}{2}\left(1-\frac{DDV_i\cdot DDV_j}{\left|DDV_i\right|\left|DDV_j\right|}\right)\right);\forall i\neq j;i=1,2,\ldots N \quad (5)$$

The PGD map gives us a baseline which can be used along with the results from the directional TBM in Section 2.1 to interpret how the directionality of growth changes with age and development. Therefore, we propose to first compute the most common growth direction at each tissue location across the population being studied and then analyze how directional growth is varying with respect to this direction at each location.

If a PGD cannot be clearly established, i.e. the eigenvalues are not well-separated at many locations, the study can be done on each of the 3 directions separately. Three deformation direction maps are formed and are studied individually. After being tested individually, the three significance maps are combined using an OR method or the fisher test.

3. Experiment

To illustrate the properties of the proposed descriptors, we have used a set of simulated image volumes. A reference image (RI) of size 256 × 256 × 128, with 0.5 mm isotropic resolution was simulated. The foreground of the RI contained an ellipsoid with equatorial radii of 30 mm and 60 mm and polar radius of 20 mm. We added the following deformation and shape changes to the RI to form various test images (TI) (as shown in Figure 2):

- **TI1** Anisotropic volume increase: The equatorial radius along the y direction was increased to 35 mm to simulate volume increase corresponding to directional elongation of the Jacobian tensor.
- **TI2** Isotropic volume increase: The radii along all three directions were increased to (45, 75, 35) mm.
- **TI3** Anisotropic volume and shape change: The RI was rotated by 45° along the z-axis and the ellipsoidal radii were changed to (30, 35, 20) mm.

The test images include all the basic elements of deformation, including 3-D isotropic expansion and contraction, and 1-D and 2-D elongations. Any local brain shape change can be explained as a combination of these elements.

In any TBM study, the suitability of a morphometric measure to capture local changes in the dataset is dependent on the registration model used. In order to best understand the properties of the proposed measures, we used it in combination with a suitable registration method. Also, the absence of ground truth for all TBM applications makes validation of new measures challenging. In the current experiments, the availability of the original deformations facilitates a complete picture of mechanics of the proposed morpho-metric measures. Each of the TIs was registered to the RI using a symmetric, pairwise registration method. The registration method estimates a pair of unbiased, dense deformation fields that align the two images to a common or average space. The average distance from each point in the common space when mapped to each of the images is forced to be zero. The deformation fields are calculated by iteratively minimizing the squared difference between the intensity boundaries of the images and the common space using gradient descent refinement. In order to enforce diffeomorphic transformation during alignment, a single-level Gaussian smoothing kernel [42] [29] was used for regularization. The deformation fields were used to compute the Jacobian tensor maps for each RI-TI pair. The DDV maps corresponding to the deformation of each TI-RI pair were computed as described in Section 2.1. Figures 3–5 show the DDV maps (of each pair of registrations between the RI and the TIs) overlaid on the spatially normalized average and displayed using RView software[1]. Figures 3–5 (b) show that voxel-wise volume changes, resulting from registration of two images, occurs along specific directions. As with any deformation based statistical descriptors, the properties of the DDV are determined by the registration model and the associated regularization method. This accounts for the discrepancy between changes at image boundaries that seem uncorrelated to the actual global difference between the two images being registered (in Figure 3).

Figure 6 shows the various stages of decomposition of the deformation tensor to compute the DDV vectors. The vectors computed from the positive root of the Cauchy-Green tensor (CGT) correspond to the primary eigen direction of the stretch component of the deformation tensor (namely the vector e_i in Figure 1). The final DDV which includes both stretch and rotation information (corresponding to vector υ_i in Figure 1) is shown in the left column. Figure 6 also illustrates the advantage of using the proposed statistical metrics over those derived from CGT [27] [47]. Figure 6 (c) shows a region (denoted with a yellow oval) where the primary direction of deformation changes significantly upon including the whole Jacobian tensor as opposed to only the positive root of the CGT. We would like to note that the proposed metrics better capture the progressive change along the image boundaries by including both stretch and rotation information.

4. Application – Early fetal brain growth

4.1. Fetal subjects and image acquisition

The following experiments were performed using 40 clinical scans of 38 fetuses at gestational ages (GA) ranging from 20.57 to 27.86 weeks GA, estimated by last menstrual period. The mothers were referred for MRI of the fetal brain due to questionable findings on prenatal ultrasound, a prior abnormal pregnancy, or volunteered for scans as part of studies at UCSF. All women had normal fetal MRI. The subject population contains 19 females and 19 males. The mean delivery age was 39.3 weeks GA (37.4 – 41.57 weeks GA). The imaging study has IRB approval and complies with NIH human subject guidelines. Clinical MR imaging was performed on a 1.5T scanner (GE Healthcare, Milwaukee,WI) using an eight-channel torso phased-array coil. Multiple stacks of single-shot fast spin- echo (SSFSE) T2 weighted slice images (in plane pixel size of 0.5 mm × 0.5 mm, thickness 3 mm, no gap)

[1] http://rview.colin-studholme.net

were obtained in the approximately axial, sagittal and coronal planes with respect to the fetal brain. All slice images were acquired in an interleaved manner to reduce saturation of spins in adjacent slices. The MR sequence parameters (repetition time TR = 3000 – 9000ms, echo time TE = 91 ms) were originally designed for clinical scans. To account and correct for spontaneous fetal movement during scanning, all image slices in the slice stacks of a subject were registered using the slice intersection motion correction (SIMC) technique [21] and reconstructed into 3D volumes with isotropic voxel size of 0.5 mm. The SIMC method has been validated using 100 synthesized datasets and 45 clinically acquired datasets. The method has shown to recover fetal motion between slice acquisitions of up to 15 mm of translation and 30 degrees of rotation with subvoxel accuracy. The 3D volume was reconstructed by gradient weighted Gaussian averaging, where voxels were selectively weighted by the acquisition quality and compounded into a 3D volume that is consistent with each of the 2D slices.

4.2. Automatic tissue segmentation

Using manual segmentations of 30 subjects, we created a spatiotemporal atlas of MR intensity, tissue probability, and shape of the fetal brain [14]. Using this atlas, a synthetic age-specific MR intensity template and an age-specific tissue probability map were generated for all 40 subjects used in this study. Each subject MRI was aligned to the age-matched MR template using a sequence of global linear registrations driven by maximization of the correlation coefficient between the age synthesized MRI and subject MRI intensities [41], followed by multiple elastic deformations driven by maximization of mutual information [46] within a fixed mask. Based on the inverse of the estimated spatial transformation, the age-matched tissue probability map was aligned with the subject MRI and used as a source of spatial priors for automatic atlas-based expectation-maximization (EM) segmentations of developing brain tissues [15]. The reconstructed volumes were automatically segmented into regions of the cortical plate (CP); subplate (SP), intermediate zone (IZ), and deep gray nuclei (DG); germinal matrix (GMAT); and ventricles (VENT) (Figure 7b)).

4.3. Groupwise registration

Deformation based morphometric brain studies require that all subject anatomies be spatially aligned so as to bring subject anatomies into the same anatomical coordinate system. For fetal morphometric studies, the optimal registration method should be template-free to avoid introducing a shape bias in the significant range of anatomies being studied. To this end, we used an unbiased groupwise registration method to coalign the tissue maps of the subjects being studied [34]. The registration method simultaneously estimates an unbiased, minimum deformation population average and diffeo-morphic transformation to each of the subjects being studied.

Fetal MR registration presents a few unique challenges which were addressed as follows:

Changing tissue contrast The developing fetal brain exhibits significant MR tissue contrast change with age. In order to avoid the possibility of bias introduced by such changing contrasts, we took the approach of aligning tissue label maps derived from automated segmentation, rather than aligning the raw MR image values directly.

Transient tissue types The fetal anatomy also contains transient tissue types that change in volume across age groups; specifically regions of GMAT and subplate are more visible on MRI in the beginning of this period (20 wks GA) but not visible in many brain regions later in the developmental period (27 weeks GA). The inconsistent tissue boundaries would introduce artifactual deformations between

anatomies as the algorithm attempts to account for the missing tissue classes in older anatomies. In order to compute meaningful diffeomorphic transformations between the anatomies, we combine the tissue classes to exclude inconsistent tissue boundaries. This was achieved by combining the transient tissue classes, corresponding to the germinal matrix, the intermediate zone, subplate, and subcortical gray matter, into a not cortical plate (NCP) tissue label (Figure 7b).

The groupwise registration is initialized with a linear registration of the NCP region of every subject to a single, average NCP tissue map [15]. The registration then estimates a set of unbiased, dense field deformations that minimize the mean square difference between the tissue label maps (CP, NCP, VENT) of each subject to the current average tissue label map (CP, NCP, VENT) for the group. Using an iterative gradient descent optimization, the squared difference in tissue labels between the current average and each individual's tissue map is summed over each tissue class, then minimized with respect to the displacement vector at each voxel. To ensure spatially differentiable mappings, a multi-level, Gaussian smoothing [42] [29] operator was used to regularize the deformation fields during alignment. A 2 mm Gaussian kernel was used at the first level to capture larger-scale shape differences and then a 1 mm Gaussian kernel was used to capture the smaller-scale and more local shape changes. A composition of a sequence of two of these diffeomorphic mappings, each characterized by a vector field of displacements (Figure 7c), from the average anatomy to each subject was estimated. The regularization factors were chosen experimentally so to enforce numerically diffeomorphic mapping during registration.

In order to validate the accuracy of the registration process, we used a subset of subjects which formed a representative age group for which manual segmentations were also available. These subjects were aligned using a combination of automatic segmentation and the groupwise registration method presented in this paper. The computed transformations were used to map the manual segmentations into the resulting average space, thus providing an independent measure of tissue alignment. The resulting overlap of the manually segmented regions in the common space was evaluated with DSC coefficients of 0.84 ± 0.02 for the CP and 0.94 ± 0.01 for the NCP. This was comparable to the underlying differences between manual and automated tissue segmentation, indicating that the groupwise registration had resolved the majority of true differences in anatomy. In addition, we confirmed that all deformations remained diffeomorphic for these regularization parameters.

4.4. Directionality of growth from TBM

For each subject, the Jacobian matrix maps were computed, from the resulting deformation fields, to quantify the pattern of deformation required to spatially normalize individual anatomies. For each subject, we computed the DCM maps from which DDV maps were extracted. An illustration of the DDV maps for a representative subject is shown in Figure 7. Using the DDV maps, we performed multivariate, multiple linear regression on the population with age as the independent variable and the directional coefficients as the dependent variables. The regression coefficients were tested for statistical significance. The growth directions are specified in the initial orientation of the average anatomical target space (axial slices with respect to a fetal brain). Among the approaches that can be used to represent growth directions, the artificial Cartesian scanning coordinates allows us to model anisotropic brain growth within a framework that is easy to understand and interpret. Regions with significant age-related changes in growth direction are shown overlaid on the spatially normalized average MRI and displayed using RView software.

We also computed, using the DDV maps, a PGD map for the subject population.

4.4.1. Group Comparison using DDV – Asymmetries in Growth Direction—

Here, we present an example of using DDV to detect group differences by examining the emergence of asymmetries in fetal brain development. We performed an additional TBM analysis that used a symmetric groupwise nonrigid registration of the tissue maps that also accounted for differences in anatomy on each side of the brain. This was performed by reflecting each of the tissue maps along the sagittal midline (longitudinal fissure) and then registering the original and reflected brains collectively to form a single symmetric average brain shape from the group. We then tested for age-consistent differences in directional volume change between the left and right hemispheres, while accounting for linear growth rate in the group. Permutation testing was used within a brain mask of the right hemisphere to correct the asymmetry maps of significance for multiple comparisons. Positive significant differences indicated greater directional volume in the right hemisphere compared to the left and vice versa for negative values.

4.5. Results and Discussion

In this paper, we have shown that the anisotropic growth that occurs during fetal brain development can be quantified using the proposed descriptors. By using these descriptors in conjunction with the TBM framework, we have detected significant changes in the direction of anisotropic growth in the age interval being studied. Significant changes in direction of growth occur primarily in the cortical plate at locations corresponding to the formation of primary sulci. When the direction of cortical growth at any sulcus changes rapidly, it occurs in conjunction with change in direction of growth in the underlying cerebral mantle.

Figure 8 shows a distinct spatial pattern in the PGD for the age range studied. The parietal and occipital regions of cerebral mantle, near the mid-line, show a strong growth along the anterior-posterior (A-P) axis during this period. Along the cortical plate, PGD alternates between superior-inferior (S-I) and right-left (R-L) axis corresponding to the formation of sulci and gyri respectively. Regions of the cerebral mantle underlying locations of sulcal formation show a predominant growth along the S-I axis to accommodate changes in tissue distribution at the sulci and gyri. The ventricles do not show a distinct direction of growth as during this period in fetal brain development, the ventricles do not change significantly in absolute size as the brain expands in volume around them [35, 13].

Figures 9 – 11 show the regions where directional growth has changed significantly with age. The regions showing significant changes correspond to regions of major cortical folding. The largest clusters of significant voxels occur at the Sylvian fissure (Fig. 9) where the significant acceleration of growth along the R-L axis and deceleration along the S-I axis indicate deepening of the fissure. As marked by the dotted circle, we see that the combination growth acceleration along the R-L axis and deceleration along S-I axis at the superior aspect of the temporal lobe results in closing of the Sylvian fissure [6, 1, 32]. To accommodate these changes in the cortical regions, we see that the cerebral mantle underlying the insular region is being “stretched” along the S-I axis, since growth along the R-L axis is restricted by neighboring structures. This combination of directional growth may be likened to the ultrasongraphy-based characterization of the temporal operculum “overriding the insula” by progressing from a 45° angle with the insula to a rounded gyrus that covers the posterior half of the insula in the axial plane [32].

In Figure 10, the white arrow indicates the location of the developing central sulcus. Similar to the Sylvian fissure, the R-L growth has significantly increased while S-I growth shows decrease at this sulcus. In contrast, the appearance of the inter-hemispheric fissure (shown by the dotted circle in Fig. 10) is characterized by accelerated expansion of the cerebral mantle in the S-I direction paired with deceleration along the R-L axis.

At the choroidal fissure, in Fig. 11, we notice a significant deceleration in growth along the R-L axis with no significant acceleration in either of the other two directions. This corresponds to the apparent shrinkage of the choroidal fissure with respect to surrounding tissues because by 19 weeks GA the fissure has reached its mature form [6].

In addition to regions of cortical folding, another region showing a large cluster of significant voxels occurs at the hippocampus. In Fig. 12, we see that formation of the hippocampus is associated with accelerated growth along the R-L axis while growth along the S-I axis shows deceleration. Infolding and laminar organization of the hippocampus is established between 18 and 21 weeks GA [19, 20]. Further growth of the hippocampus may be a result of lateral expansion of the subfields, which would result in R-L expansion, but this is yet to be shown by histological study.

Considering the PGD in Figure 8 together with directional changes in growth indicated by Figures 9 – 12, we see that brain growth is characterized by spatially distinct variations in growth directions. In some regions this directionality does not change significantly as the fetus matures. For example, the cerebral mantle which showed a very pronounced growth along the A-P axis in Figure 8 does not exhibit significant accelerations and decelerations in any direction in the period of growth considered for this study. Major shape changes in the cortex occur due to significant changes in directional growth at sites of sulci and gyri. The effect of these changes in direction on underlying tissue is determined by the rate of those changes in the age range being studied. For example, the operculization of the Sylvian fissure and changes at the inter-hemispheric fissure occur at a rapid rate and thereby the change in directionality in both the CP and the underlying cerebral mantle are captured. During the same age range, the rate the choroidal and central sulci show a slower rate of growth in the same age range [16], therefore the changes in the underlying cerebral mantle are not significantly higher than the surrounding tissue.

4.5.1. Group Comparison using DDV – Asymmetries in Growth Direction—By comparing directional growth rates across the hemispheres, we detected local asymmetries in the peri-sylvian region and the medial frontal lobe of the developing brain (Figure 13). We observed that rightward asymmetries are strongly correlated with significant increase in growth along the R-L axis. This directional growth asymmetry is coupled with rightward volumetric growth asymmetry in the temporal operculum, as shown in previous study of the same population [34]. The congruent findings show that the faster growth in this region on the right hemisphere is due to greater expansion along the R-L axis. Ex vivo studies of fetal brain development have consistently demonstrated that this fissure develops earlier in the right hemisphere [6, 1] and the DDV shows where the opercularization process is occuring significantly faster.

The emergence of medial frontal asymmetries manifests as greater growth along the R-L axis paired with slower growth along the S-I axis in the right hemisphere. The asymmetric contribution along the R-L axis may be attributing to the phenomenon known as torque [45], in which the right anterior frontal lobe is larger than the left and protrudes over the skull cavity midline in the mature brain [25].

4.6. Comparison to results from scalar TBM models

Figure 14 shows an overview of results from the proposed directional TBM method and scalar, volume based morphometric model that study fetal brain growth, at an identical age range [34]. Both the scalar and the proposed directional growth models examine the growth patterns associated with gyrogenesis along much of the developing cerebral mantle. The scalar model detects regions where statistically significant changes in local volume occur in the age range being studied. By including directional information, we were able to specify

the axis along which brain dimensions change resulting in volume changes. Localizing the axis of dimension change allows us to characterize interconnected changes associated with gyrification across tissue types. For example, the findings from the current DDV model and the volume growth rate model of the same dataset [34] showed bilateral differential growth at the emerging cingulate sulcus in both the cortical plate and underlying subplate (Figure 9 and Figure 14 (b)). The tissues that would be associated with the crest of the adjacent gyri do not share the pattern of increased growth rate. Importantly, the DDV indicates a cle ar increase in growth rate along the right-left axis, which corresponds to increasing depth of the central sulcus that affects more than just the shape of the cortical surface. In conjunction with the growth rate model, the current directional TBM model allows an estimation of the rate of sulcal deepening to then be made over multiple tissues.

Using diectional information in conjunction with scalar TBM analysis also enhances our understanding of the appearance of structural lateralization. For example, both scalar [34] and directional analysis of the same dataset used here showed significant growth rate asymmetry in the peri-Sylvian region. Specifically, the right superior temporal gyrus and temporal operculum grew faster in the right hemisphere and the inferior frontal gyrus and frontal operculum expanded faster on the left. Similarly, local mean curvature analysis detected asymmetries in cortical folding that match the growth rate spatial pattern [16]. Together these findings suggested the Sylvian fissure hemispheric asymmetries (flat on left, posteriorly arched on right) observed in the mature brain [25, 18] actively form during primary gyrogenesis and that the right hemisphere undergoes cortical folding earlier than the left. Results from the current directional analysis of asymmetry shows that this reliable hemispheric asymmetry is only significantly associated with greater right-left expansion in the posterior part of the temporal operculum (Figure 13). The directional information illustrates that the right Sylvian fissure is emerging sooner by expansion of the temporal operculum laterally, rather than by differences in growth direction along the insular region. The right-left acceleration in the temporal region, in contrast to the frontal or parietal, may also be a driving factor in the shape differences of the Sylvian fissure. Modeling the mechanisms by which the fissure reaches mature form would necessitate extending the directional TBM model to term, when the contributions of latter emerging gyri could be evaluated.

4.7. Limitations

When using structural MRI (T1W or T2W), regions of uniform tissue result in regions with uniform intensity and therefore lack contrasting features for registration. This limits the interpretation of results from any brain volume mapping technique in regions deep within uniform tissue. In the absence of dense features, such as those provided by diffusion tensor imaging for TBM [37], the resulting maps of volume differences between anatomies reflect an optimally smooth representation of deformations that must occur within the region to create the observed differences in the surrounding boundaries (e.g., thickening, elongation, folding). When using T2W MRI data for brain volume mapping, the final deformation maps are inevitably linked to the regularization method used during the registration process.

In both the current study and other studies that use similar methods, the significant regions detected in the cerebral mantle are in agreement with published literature (from histology and other methods). This provides a validation of the claim that even in regions where the regularization effects are most pronounced, characteristic patterns detected by this method are still useful in understanding the process of fetal brain growth. Most TBM studies (fetal brain or otherwise) include some level of regularization without it influencing the final outcome of the study. Therefore, the dependence of the deformations on the regularization does not however limit the usefulness and statistical significance of the characteristic volume change patterns extracted by the TBM approach.

5. Conclusion

In this paper, we have used two novel morphometric descriptors that allow us to characterize anisotropic growth associated with fetal brain development. The two complementary metrics allowed us to model common patterns in directional growth associated with human, fetal brain development during mid-gestation and also detect regions showing significant deviations from these patterns as the brain matures. By including directional information along with volume growth, we have for the first time simultaneously modeled both volume and shape changes associated with primary gyrogenesis. The inclusion of directional growth information with standard TBM allowed us to model both cortical changes and the associated growth patterns on the underlying cerebral mantle that occur during gyrogenesis. Unlike other morphometric descriptors, growth patterns are specified in terms of the Cartesian anatomical co-ordinate system, whose ease of interpretation increases the clinical value of our method. We have also used the proposed metrics to measure directional asymmetry associated with the emergence of structural lateralization in the developing brain. While hemispheric asymmetry was detected in other scalar TBM models, we have for the first time, reliably modeled the series of interconnected, local changes associated with lateralization of this structure. This allows us to better understand the mechanism by which structural asymmetry emerges in the developing human brain.

The use of these descriptors need not be restricted to only brain development studies. Any TBM application where brain structural differences (within or between groups) arise from directional variations in tissue gain/loss can be studied using the proposed descriptors.

Acknowledgments

This research was funded by NIH/NINDS grants: R01 NS 061957 and R01 NS 055064. Imaging for this study was also partially supported by the National Institutes of Health (NIH) Grant No. K23 NS52506-03 and NIH/NCRR UCSF-CTSI Grant No. UL1 RR024131. The work of F. Rousseau was supported by European Research Council under FP7/2007-2013 Grant Agreement 207667.

6. References

1. Afif A, Bouvier R, Buenerd A, Trouillas J, Mertens P. Development of the human fetal insular cortex: study of the gyration from 13 to 28 gestational weeks. Brain Struct Funct. 2007; 212(3–4): 335–346. [PubMed: 17962979]
2. Aljabar P, Bhatia KK, Murgasova M, Hajnal JV, Boardman JP, Srinivasan L, Rutherford MA, Dyet LE, Edwards AD, Rueck-ert D. Assessment of brain growth in early childhood using deformation-based morphometry. Neuroimage. 2008; 39(1):348–358. [PubMed: 17919930]
3. Armstrong E, Schleicher A, Omran H, Curtis M, Zilles K. The ontogeny of human gyrification. Cerebral Cortex. 1995; 5(1):56–63. [PubMed: 7719130]
4. Ashburner J, Hutton C, Frackowiak R, Johnsrude I, Price C, Fris-ton K. Identifying global anatomical differences: Deformation-based mor-phometry. Human Brain Mapping. 1998; 6(5–6): 348–357. [PubMed: 9788071]
5. Batchelor P, Castellano Smith A, Hill D, Hawkes D, Cox T, Dean A. Measures of folding applied to the development of the human fetal brain. IEEE Transactions on Medical Imaging. 2002; 21(8): 953–965. [PubMed: 12472268]
6. Chi J, Dooling E, Gilles F. Gyral development of human brain. Annals of Neurology. 1977; 1(1): 86–93. [PubMed: 560818]
7. Davatzikos C, Vaillant M, Resnick S, Prince J, Letovsky S, Bryan R. A computerized approach for morphological analysis of the corpus callosum. Journal of Computer Assisted Tomography. 1996; 20(1):88–97. [PubMed: 8576488]
8. De Souza Neto, E.; Peric, D.; Owen, D. Computational methods for plasticity : theory and applications. Wiley; 2008.

9. Dubois J, Benders M, Cachia A, Lazeyras F, a Vinh Leuchter R, Sizonenko S, Borradori-Tolsa C, Mangin J, Huppi P. Mapping the early cortical folding process in the preterm newborn brain. Cerebral Cortex. 2008; 18(6):1444–1454. [PubMed: 17934189]
10. Fisher, R. Statistical Methods for Research Workers. Oliver and Boyd; 1932.
11. Gogtay N, Giedd J, Lusk L, Hayashi K, Greenstein D, Vaituzis A, Nugent T, Herman D, Clasen L, Toga A, Rapoport J, Thompson P. Dynamic mapping of human cortical development during childhood through early adulthood. Proceedings of the National Academy of Sciences USA. 2004; 101(21):8174–8179.
12. Golub, G.; Van Loan, C. Matrix Computations (Johns Hopkins Studies in Mathematical Sciences). 3rd ed.. The Johns Hopkins University Press; 1996.
13. Grossman R, Hoffman C, Mardor Y, Biegon A. Quantitative MRI measurements of human fetal brain development in utero. Neuroimage. 2006; 33(2):463–470. [PubMed: 16938471]
14. Habas PA, Kim K, Corbett-Detig JM, Rousseau F, Glenn OA, Barkovich AJ, Studholme C. A spatiotemporal atlas of MR intensity, tissue probability and shape of the fetal brain with application to segmentation. Neuroimage. 2010; 53(2):460–470. [PubMed: 20600970]
15. Habas PA, Kim K, Rousseau F, Glenn OA, Barkovich AJ, Studholme C. Atlas-based segmentation of developing tissues in the human brain with quantitative validation in young fetuses. Human Brain Mapping. 2010; 31(9):1348–1358. [PubMed: 20108226]
16. Habas PA, Scott JA, Roosta A, Rajagopalan V, Kim K, Rousseau F, Barkovich AJ, Glenn OA, Studholme C. Early folding patterns and asymmetries of the normal human brain detected from in utero MRI. Cerebral Cortex. In Press.
17. Hilgetag CC, Barbas H. Role of mechanical factors in the morphology of the primate cerebral cortex. PLoS Computational Biology. 2006; 2(3):e22. [PubMed: 16557292]
18. Hill J, Inder T, Neil J, Dierker D, Harwell J, Van Essen D. Similar patterns of cortical expansion during human development and evolution. Proceedings of the National Academy of Sciences USA. 2010; 107(29):13135–13140.
19. Humphrey T. The development of the human hippocampal fissure. J Anat. 1967; 101:655–676. [PubMed: 6059818]
20. Kier E, Kim J, Fulbright R, Bronen R. Embryology of the human fetal hippocampus: MR imaging, anatomy and histology. American Journal of Neuroradiology. 1997; 18:525–532. [PubMed: 9090416]
21. Kim K, Habas PA, Rousseau F, Glenn OA, Barkovich AJ, Studholme C. Intersection based motion correction of multislice MRI for 3-D in utero fetal brain image formation. IEEE Transactions on Medical Imaging. 2010; 29(1):146–158. [PubMed: 19744911]
22. Kochunov P, Castro C, Davis D, Dudley D, Brewer J, Zhang Y, Kroenke C, Purdy D, Fox P, Simerly C. Mapping primary gyrogenesis during fetal development in primate brains: high-resolution in utero structural MRI of fetal brain development in pregnant baboons. Frontiers of Neuroscience. 2010; 4(3):20.
23. Lancaster J, Kochunov P, Thompson P, Toga A, Fox P. Asymmetry of the brain surface from deformation field analysis. Human Brain Mapping. 2003; 19(2):79–89. [PubMed: 12768532]
24. Lee J, Fonov V, Evans A. Mapping brain growth of early childhood using deformation based morphometry. Neuroimage. 2009; 47(Supplement 1):S153–S153.
25. LeMay M. Morphological cerebral asymmetries of modern man, fossil man, and nonhuman primate. Annals of the New York Academy of Sciences. 1976; 280:349–366. [PubMed: 827951]
26. Lenroot RK, Gogtay N, Greenstein DK, Wells EM, Wallace GL, Clasen LS, Blumenthal JD, Lerch J, Zijdenbos AP, Evans AC, Thompson PM, Giedd JN. Sexual dimorphism of brain developmental trajectories during childhood and adolescence. Neuroimage. 2007; 36(4):1065–1073. [PubMed: 17513132]
27. Lepore N, Brun CA, Chou Y-Y, Chiang M-C, Dutton RA, Hayashi KM, Luders E, Lopez OL, Aizenstein H, Toga AW, Becker JT, Thompson PM. Generalized tensor-based morphometry of HIV/AIDS using multivariate statistics on deformation tensors. IEEE Transactions on Medical Imaging. 2008; 27(1):129–141. [PubMed: 18270068]
28. Lund U. Least circular distance regression for directional data. Journal of Applied Statistics. 1999; 26(6):723–733.

29. Modersitzki, J. Numerical methods for image registration. Oxford University Press; 2004.
30. Nichols T, Holmes A. Nonparametric permutation tests for functional neuroimaging: A primer with examples. Human Brain Mapping. 2002; 15:1–25. [PubMed: 11747097]
31. Noll, W.; Truesdell, C. The Non-Linear Field Theories of Mechanics. Springer-Verlag; 1965.
32. Quarello E, Stirnemann J, Ville Y, Guibaud L. Assessment of fetal Sylvian fissure operculization between 22 and 32 weeks: A subjective approach. Ultrasound in Obstetrics and Gynecology. 2008; 32(1):44–49. [PubMed: 18570210]
33. Rajagopalan V, Scott J, Habas P, Kim K, Rousseau F, Glenn O, Barkovich A, Studholme C. Measures for characterizing directionality specific volume changes in TBM of brain growth. Medical Image Computing and Computer Assisted Intervention. 2010; 6362(2):339–346. [PubMed: 20879333]
34. Rajagopalan V, Scott JA, Habas PA, Corbett-Detig JM, Kim K, Rousseau F, Barkovich AJ, Glenn OA, Studholme C. Local tissue growth patterns underlying normal fetal human brain gyrification quantified in utero. Journal of Neuroscience. 2011; 31:2878–2887. [PubMed: 21414909]
35. Scott JA, Habas PA, Kim K, Rajagopalan V, Hamzelou KS, Corbett-Detig JM, Barkovich AJ, Glenn OA, Studholme C. Growth trajectories of the human fetal brain tissues estimated from 3d reconstructed in utero MRI. International Journal of Developmental Neuroscience. 2011; 29(5): 529–536. [PubMed: 21530634]
36. Smart IH, McSherry GM. Gyrus formation in the cerebral cortex in the ferret. I. Description of the external changes. Journal of Anatomy. 1986; 146:141–152. [PubMed: 3693054]
37. Studholme C. Dense feature deformation morphometry: Incorporating DTI data into conventional MRI morphometry. Medical Image Analysis. 2008; 12(6):742–751. [PubMed: 18555734]
38. Studholme C. Mapping fetal brain development in utero using magnetic resonance imaging: The big bang of brain mapping. Annual Review of Biomedical Engineering. 2011; 13:345–368.
39. Studholme C, Cardenas V. Population based analysis of directional information in serial deformation tensor morphometry. Medical Image Computing and Computer Assisted Intervention. 2007:311–318. [PubMed: 18044583]
40. Studholme C, Cardenas V, Schuff N, Rosen H, Miller B, Weiner M. Detecting spatially consistent structural differences in Alzheimer's and fronto temporal dementia using deformation morphometry. Medical Image Computing and Computer Assisted Intervention. 2001:41–48.
41. Studholme C, Hill DLG, Hawkes DJ. An overlap invariant entropy measure of 3D medical image alignment. Pattern Recognition. 1999; 32(1):71–86.
42. Thirion J. Image matching as a diffusion process: An analogy with maxwell's demons. Medical Image Analysis. 1998; 2(3):243–260. [PubMed: 9873902]
43. Thompson PM, Giedd JN, Woods RP, MacDonald D, Evans AC, Toga AW. Growth patterns in the developing brain detected by using continuum mechanical tensor maps. Nature. 2000; 404(6774): 190–193. [PubMed: 10724172]
44. Thompson PM, Mega MS, Woods RP, Zoumalan CI, Lind-shield CJ, Blanton RE, Moussai J, Holmes CJ, Cummings JL, Toga AW. Cortical change in Alzheimer's disease detected with a disease-specific population-based brain atlas. Cerebral Cortex. 2001; 11(1):1–16. [PubMed: 11113031]
45. Tzarouchi LC, Astrakas LG, Xydis V, Zikou A, Kosta P, Drougia A, Andronikou S, Argyropoulou MI. Age-related grey matter changes in preterm infants: An MRI study. Neuroimage. 2009; 47(4): 1148–1153. [PubMed: 19348950]
46. Viola P, Wells WM. Alignment by maximization of mutual information. International Journal of Computer Vision. 1997; 24(2):137–154.
47. Wang W, Hoerder-Suabedissen A, Oeschger F, Bayatti N, Ip B, Lindsay S, Supramaniam V, Srinivasan L, Rutherford M, Moll-gard K, Clowry G, Molnar Z. Subplate in the developing cortex of mouse and human. Journal of Anatomy. 2010; 217:368–380. [PubMed: 20727056]
48. Zhang H, Awate S, Das S, Woo J, Melhem E, Gee J, Yushkevich P. A tract-specific framework for white matter morphometry combining macroscopic and microscopic tract features. Medical Image Computing and Computer Assisted Intervention. 2009:141–149. [PubMed: 20426106]

Highlights

- Mathematical framework to detect anisotropic volume changes associated with brain deformation
- Framework includes two novel descriptors that quantify directionality of volume change
- Used, with TBM, to model population-wide patterns in brain morphological changes
- Proposed method used to map local patterns of directional growth in fetal human brain
- Also used to map directional hemispheric asymmetry in growth

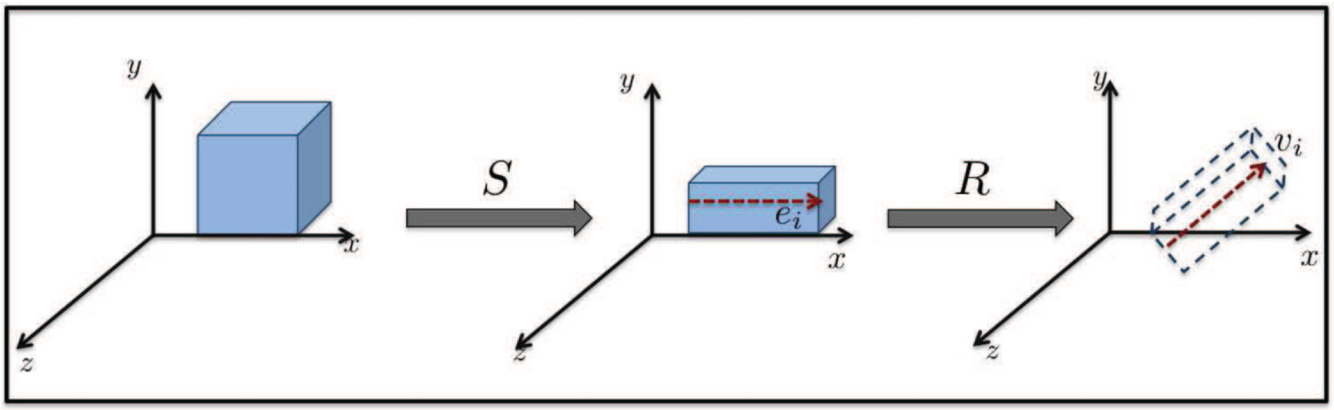

Figure 1.
Computation of deformation direction vector (DDV) from polar decomposition of Jacobian matrix

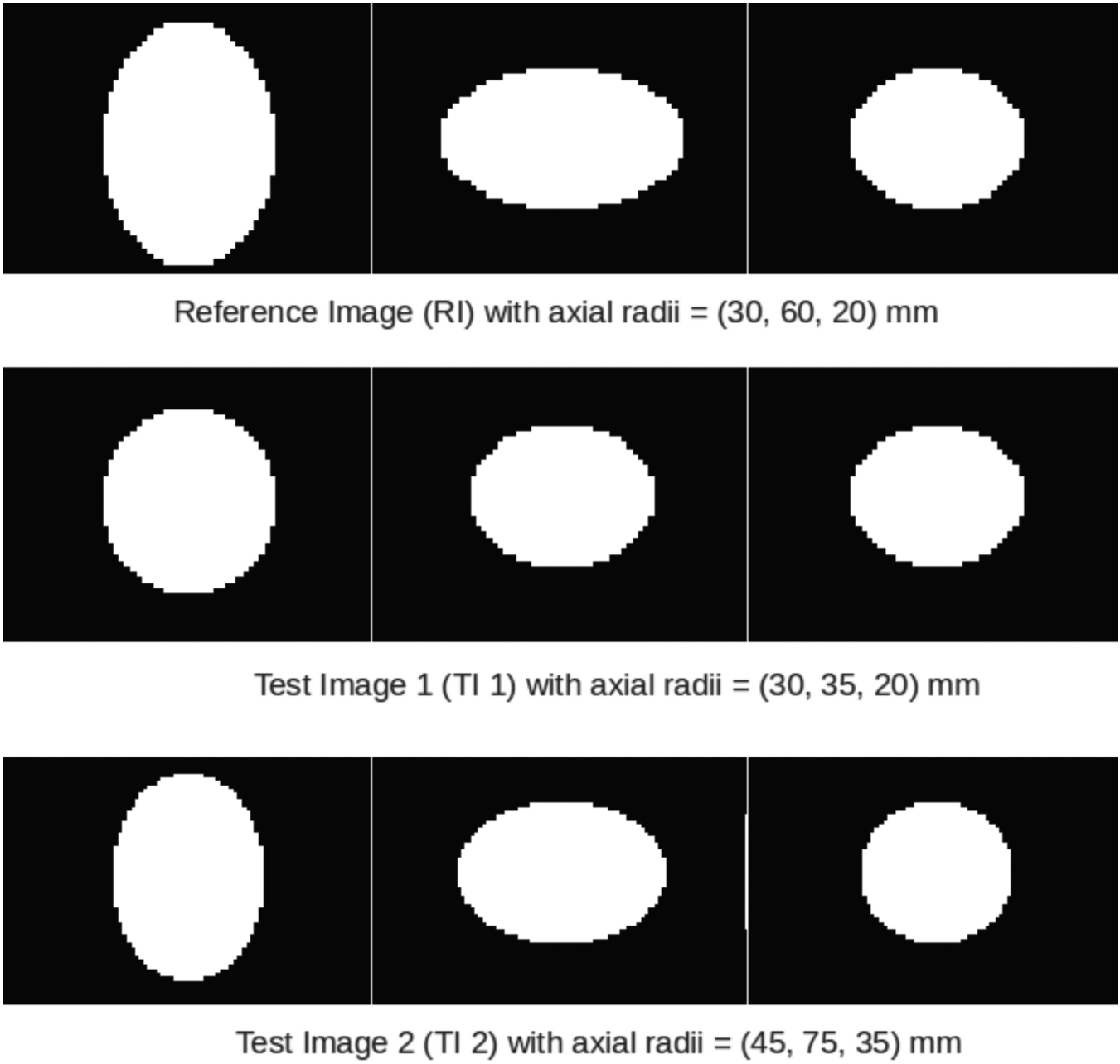

Figure 2.
Simulated Images

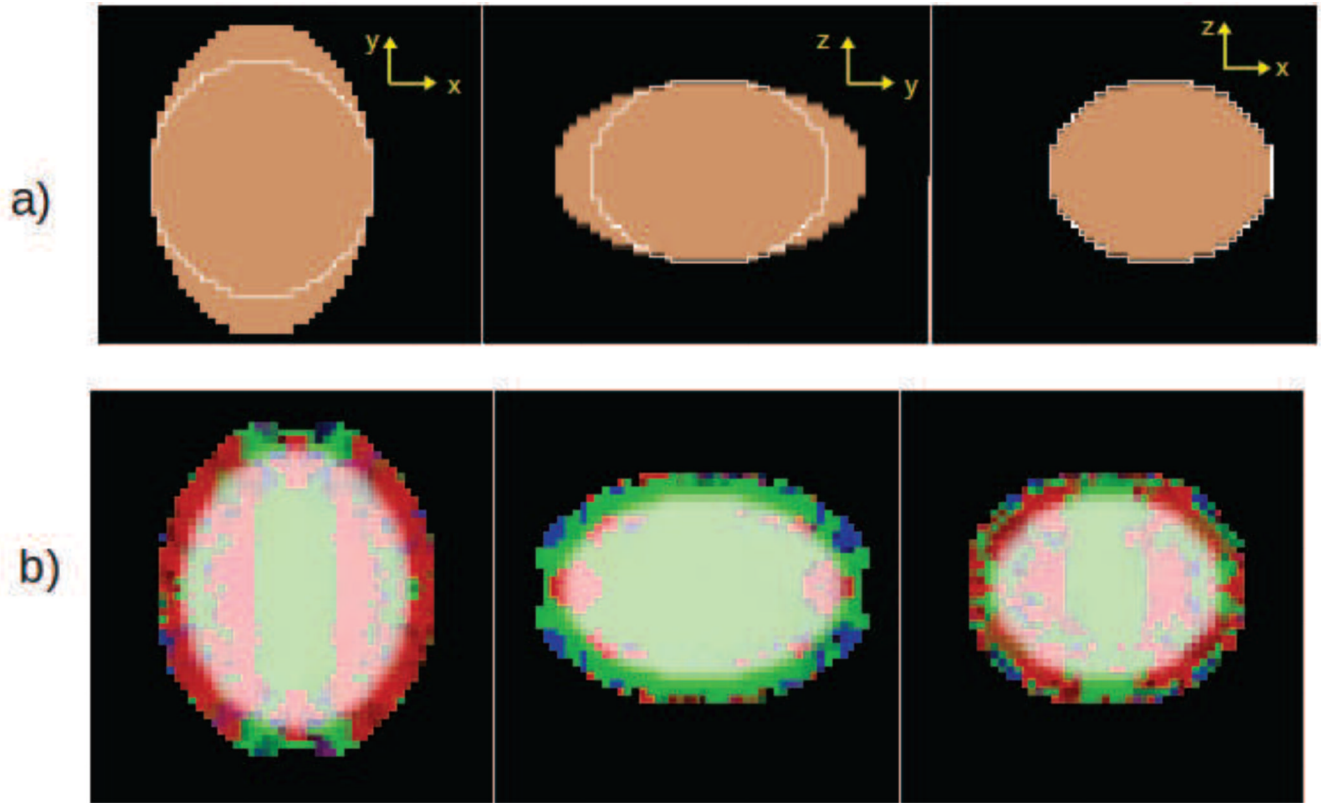

Figure 3.
a) Comparing RI (brown solid figure) with TI 1 (white contour). b) Deformation direction vector (DDV) of the deformation of TI 1 to RI overlaid on the average output (of the registration) image. The three orthogonal slices of the 3D object show that the registration resulted in changes predominantly along the Y direction. Each reference direction is represented by one color: red = X ; green = Y; blue = Z.

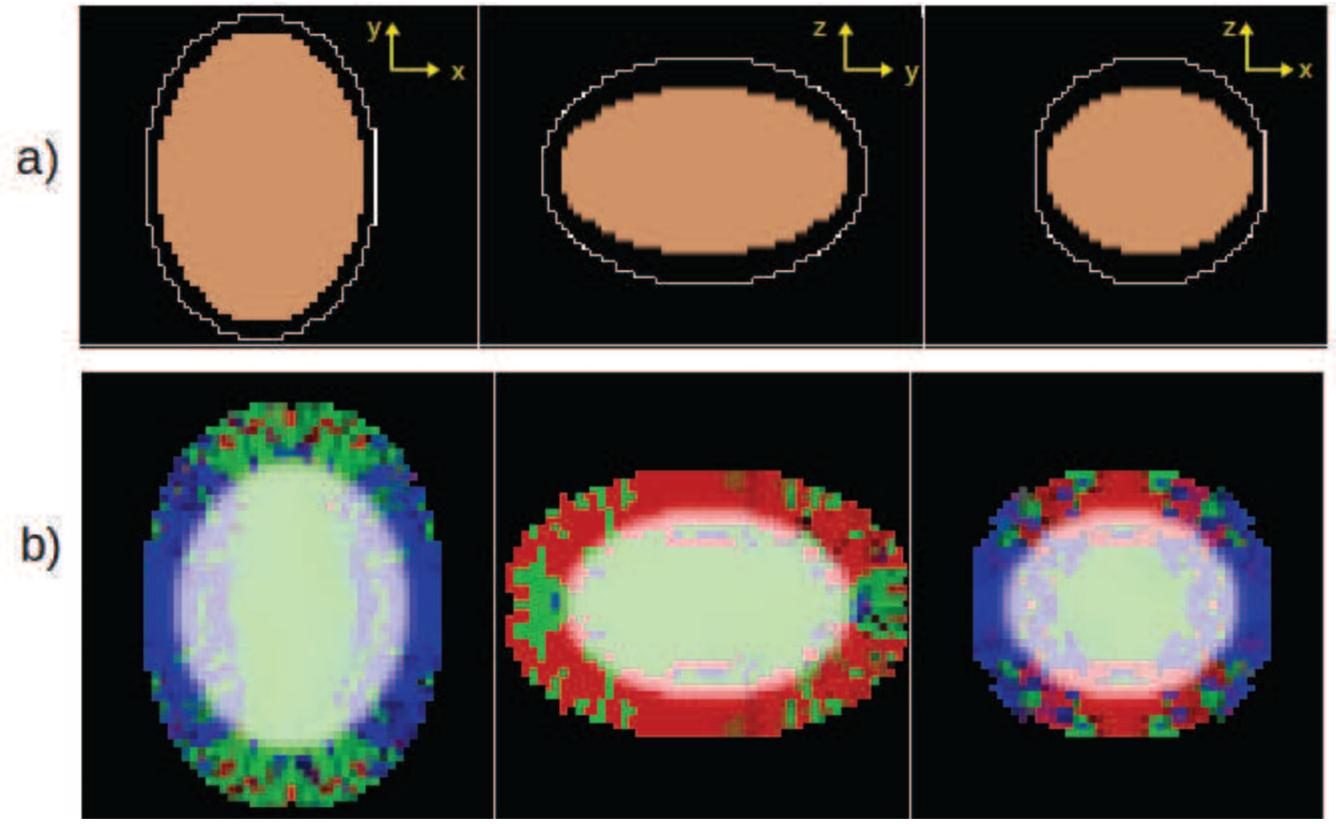

Figure 4.

a) Comparing RI (brown solid figure) with TI 2 (white contour). b) Deformation direction vector (DDV) of the deformation of TI 2 to RI overlaid on the average output (of the registration) image. The figure shows that local deformation patterns are directionally specific for two images separated by an isotropic volume increase. Each reference direction is represented by one color: red = X ; green = Y; blue = Z.

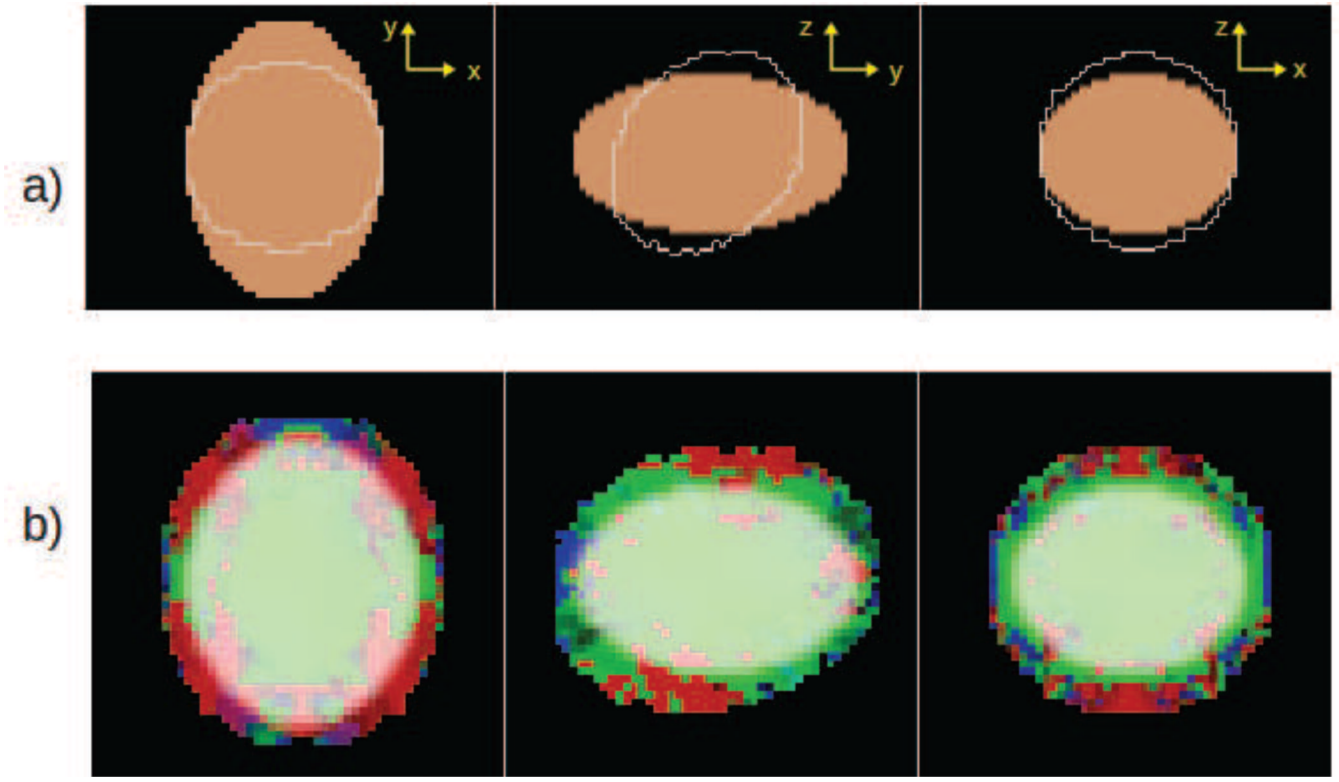

Figure 5.
a) Comparing RI (brown solid figure) with TI 3 (white contour). b) Deformation direction vector (DDV) of the deformation of TI 3 to RI overlaid on the average output (of the registration) image. We note that as the changes between the RI and TI become more complex, the directionality of volume changes become increasingly localized. Each reference direction is represented by one color: red = X ; green = Y; blue = Z.

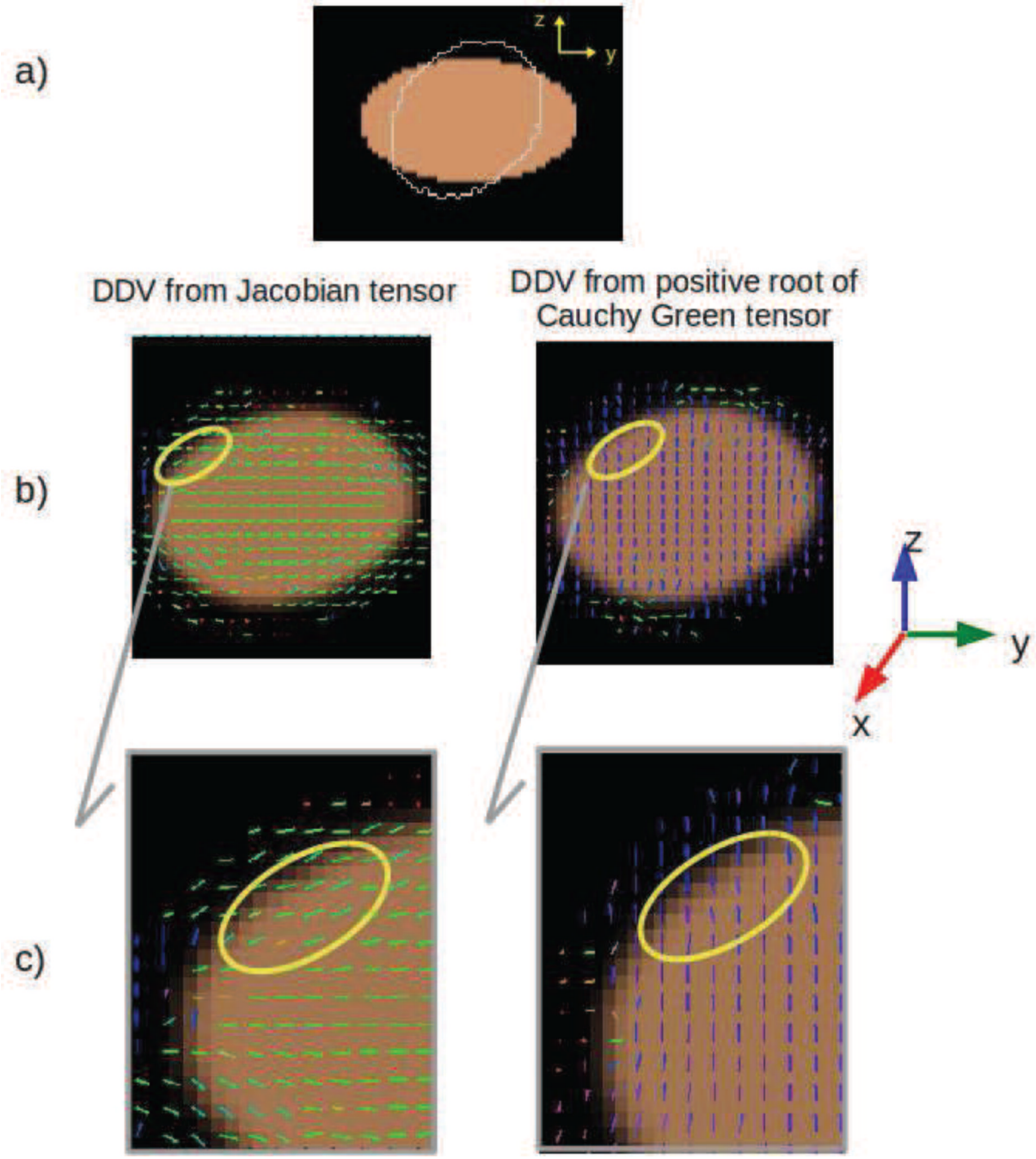

Figure 6.

a) Single Slice view comparing RI (brown solid figure) with TI 3 (white contour). b) Example to illustrate the importance of including rotational information in the Jacobian tensor. c) Each reference direction is represented by one color: red = X ; green = Y; blue = Z.

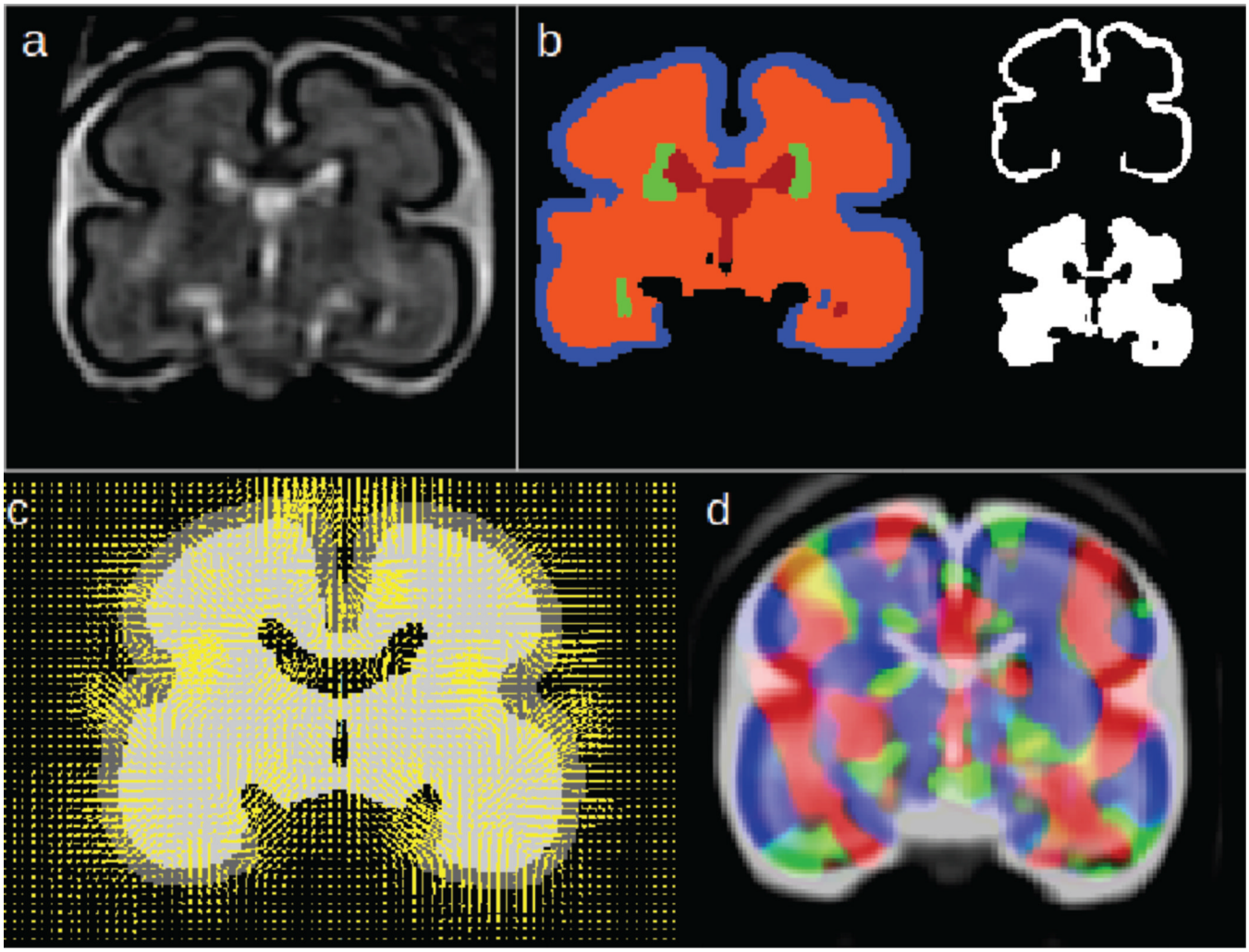

Figure 7.

Example intermediate results of processing steps for a representative subject (26.86 weeks GA). a. Original T2-weighted image. b. Automatic segmentation of the image into cortical plate (CP) shown in blue, subplate (SP) and intermediate zone (IZ) shown in orange, germinal matrix (GMAT) shown in green, and ventricles (VENT) shown in red. The segmentation is converted into tissue probability maps for CP (top right) and not cortical plate or NCP (bottom right) to exclude age-inconsistent, transient tissue boundaries. c. Deformation vector map overlaid on the population average image showing the deformation required to map the group average anatomy to the subject. d. Deformation direction vector (DDV) map computed from the deformation tensors overlaid on the average image; directional component along each reference anatomical axis is indicated by one color: red = left-right (L-R); green = anterior- posterior (A-P); blue = superior-inferior (S-I).

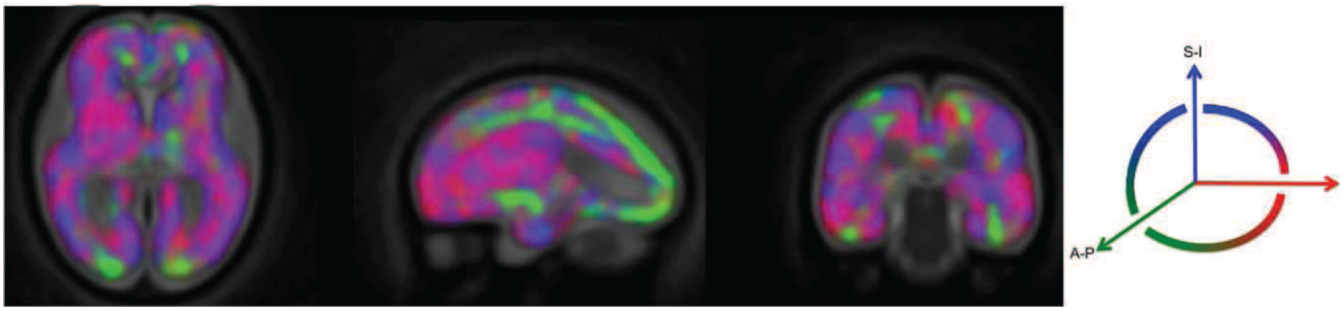

Figure 8.
Principal growth direction (PGD) vectors for the group of fetal anatomies studied. Changes along each reference anatomical axis is indicated by one color: red = left-right (R-L); green = anterior- posterior (A-P); blue = superior-inferior (S-I). The panels from left to right indicate axial, sagittal and coronal views of the brain.

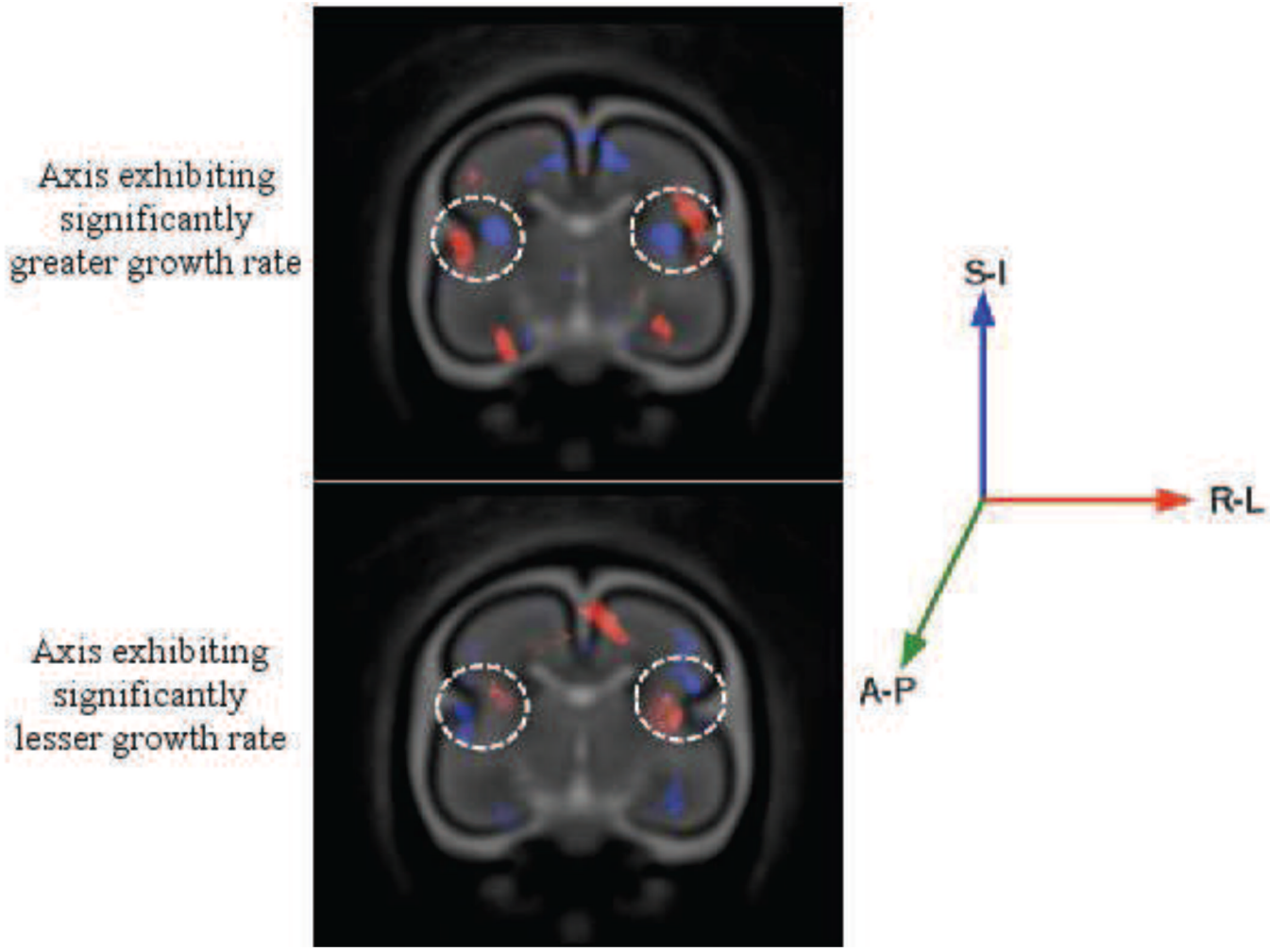

Figure 9.
Directional growth changes caused by operculization, as shown by white dotted circle. Folding causes significant changes both in the cortical plate and underlying cerebral mantle. Changes along each reference anatomical axis is indicated by one color: red = left-right (R-L); green = anterior- posterior (A-P); blue = superior-inferior (S-I).

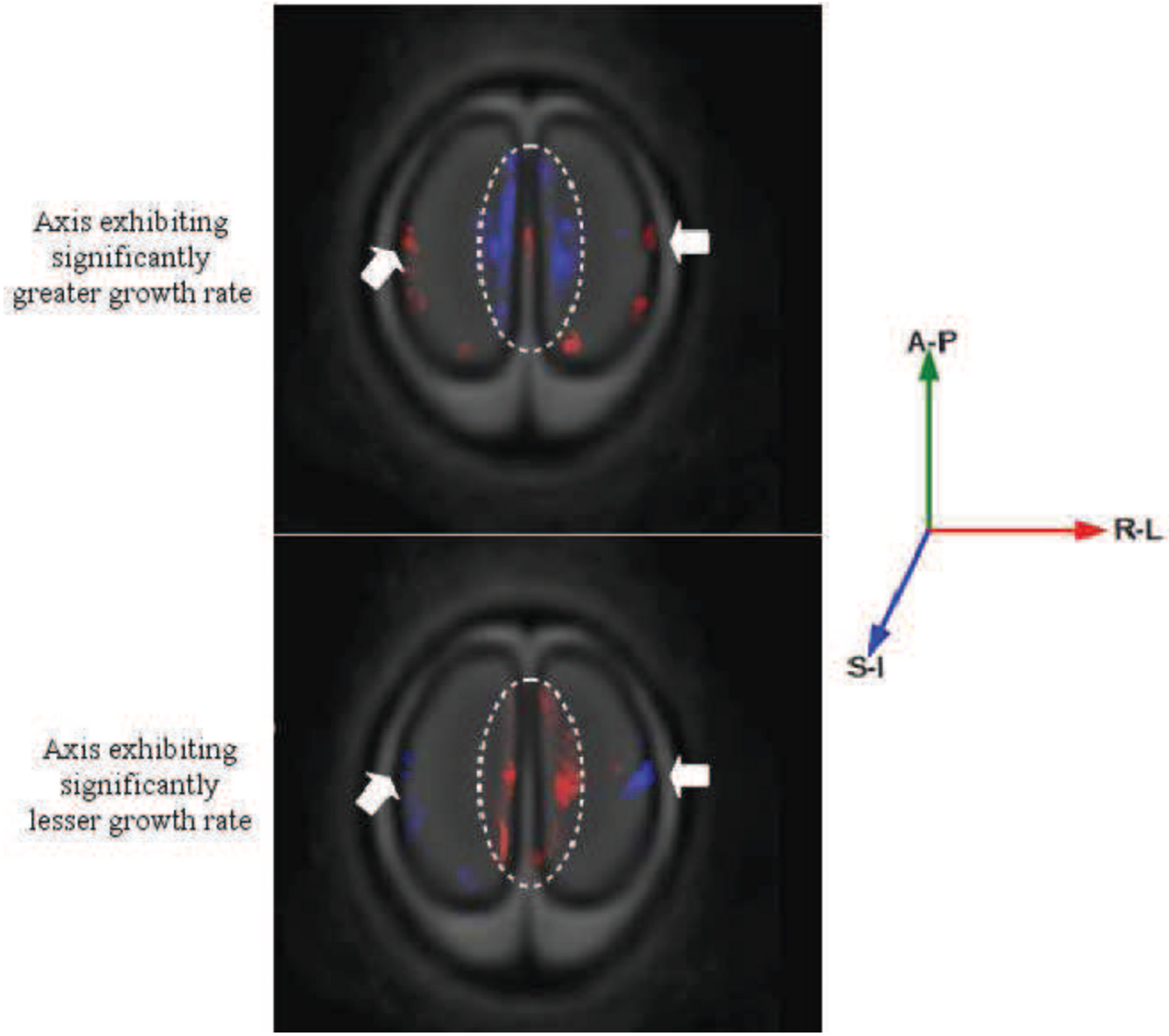

Figure 10.
Axial view showing directional changes at the central sulcus (white arrows). Along the interhemispheric fissure, the change in directional growth is more dominant at the underlying cerebral mantle (shown my dotted ellipse) than on the cortical plate. Changes along each reference anatomical direction is indicated by one color: red = left-right (R-L); green = anterior- posterior (A-P); blue = superior-inferior (S-I).

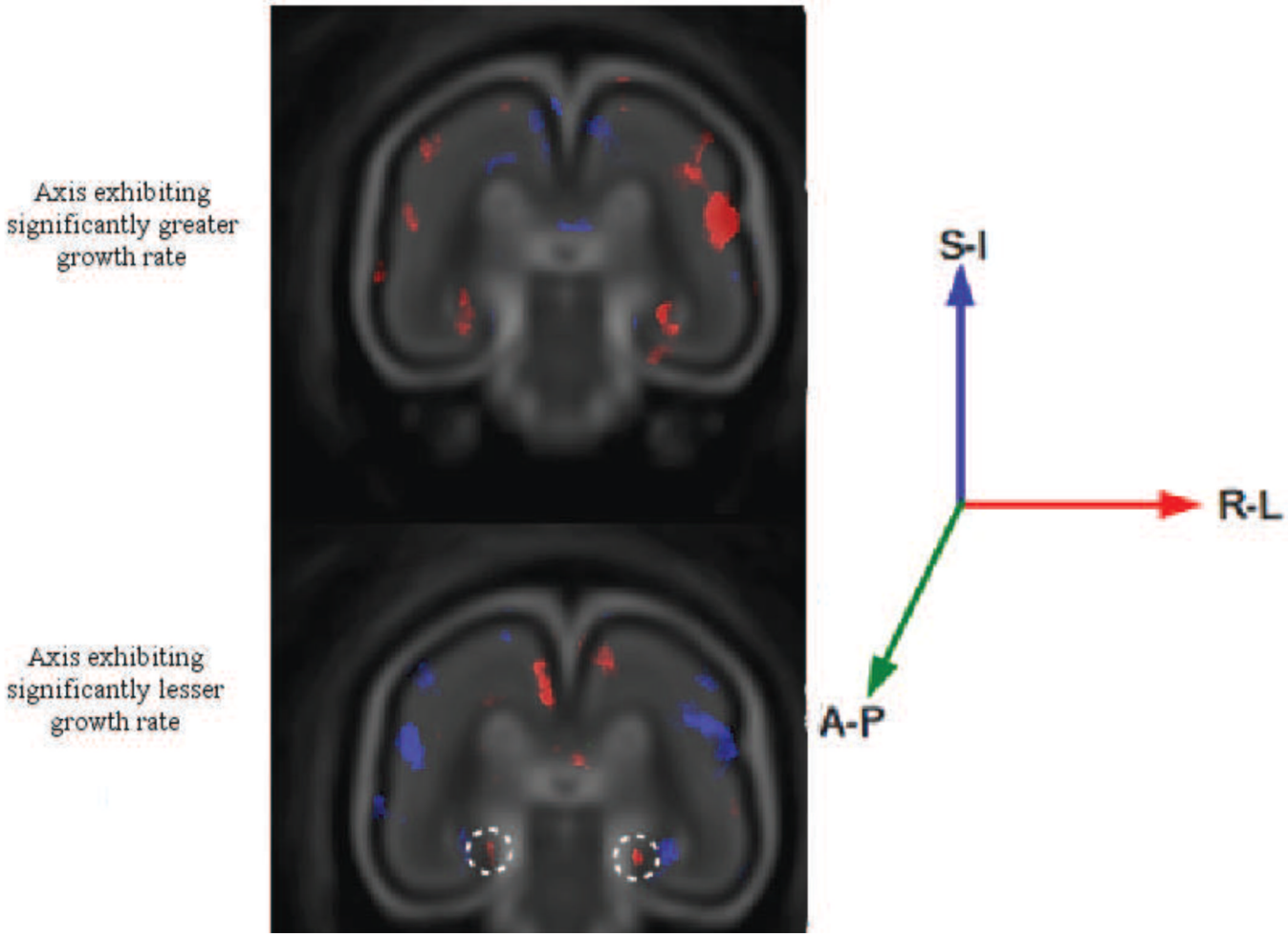

Figure 11.
Coronal view showing deceleration of R-L growth at the choroidal fissure, as shown by white dotted circle. Changes along each reference anatomical direction is indicated by one color: red = left-right (R-L); green = anterior-posterior (A-P); blue = superior-inferior (S-I).

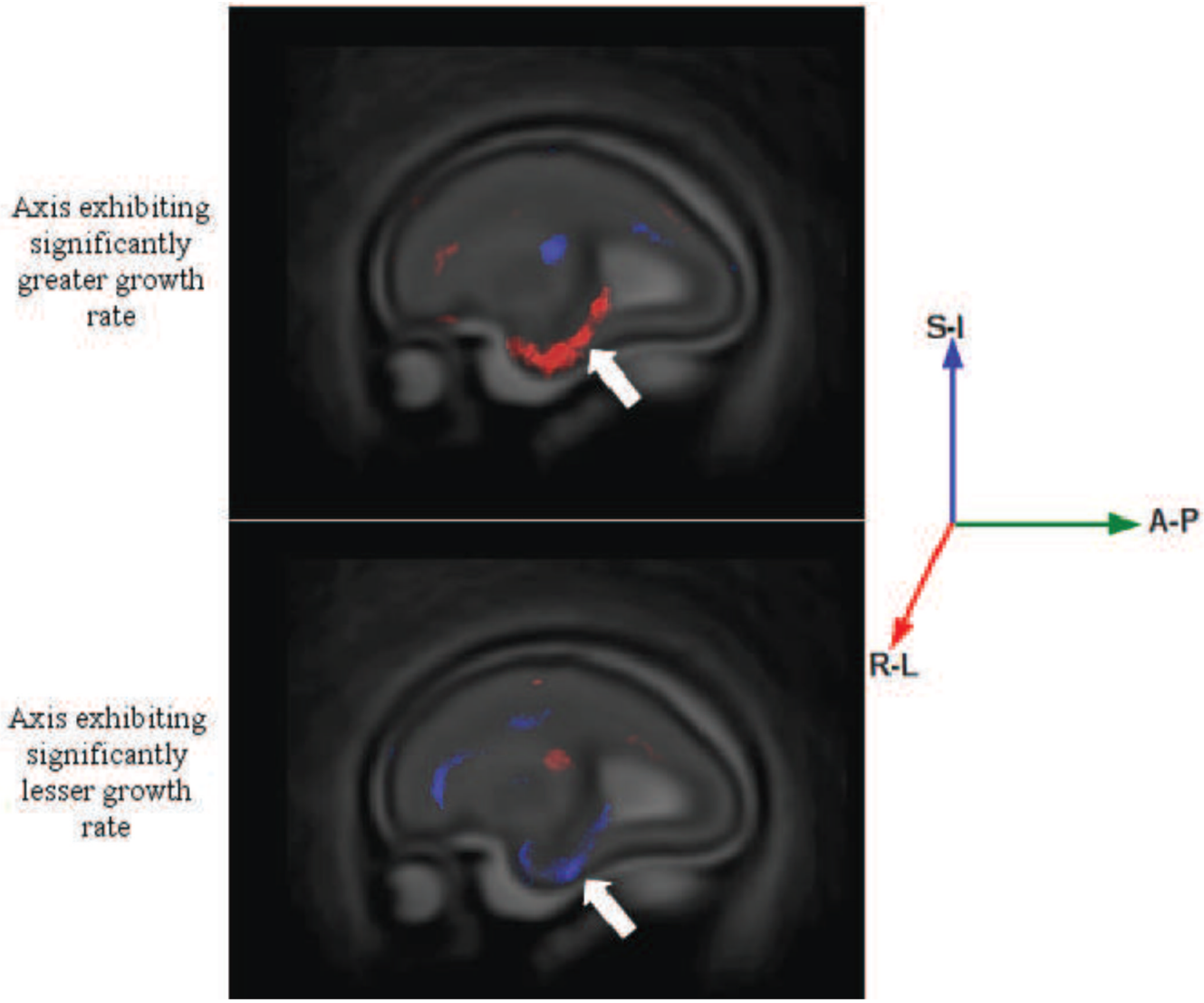

Figure 12.
Sagittal view showing the R-L expansion of the hippocampal region. The region also exhibits significant deceleration of S-I growth. Changes along each reference anatomical direction is indicated by one color: red = left-right (R-L); green = anterior-posterior (A-P); blue = superior-inferior (S-I).

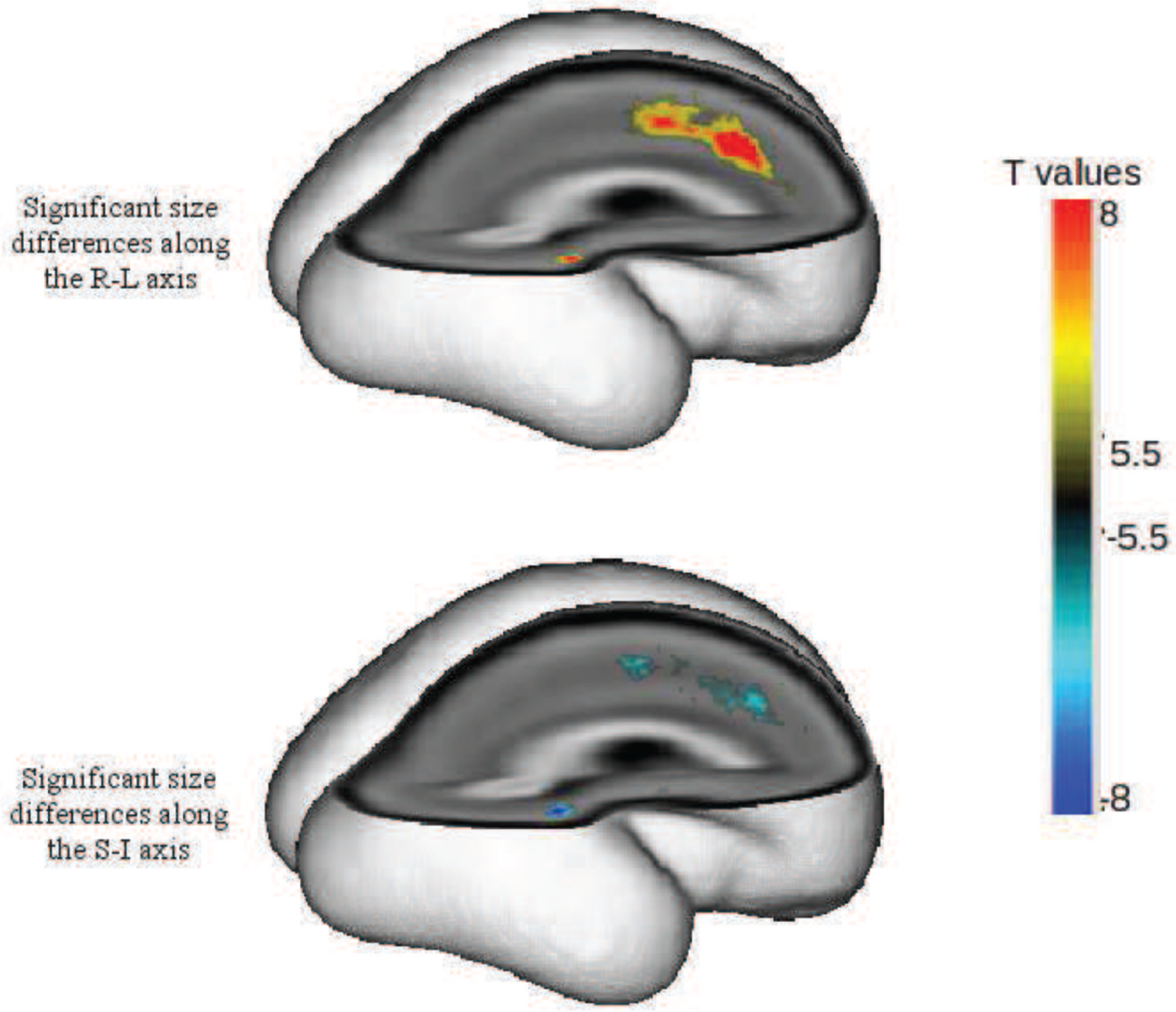

Figure 13.

T statistic maps of significant ($p \leq 0.05$, corrected) local volumetric asymmetries present from 20 to 28 weeks GA, in which warm colors indicate right hemisphere greater than left and cool colors represent left greater than right. T values are overlaid on cross-sectional slices of the right hemisphere. Positive T values indicate greater directional volume in the right hemisphere compared to the left and vice versa for negative values.

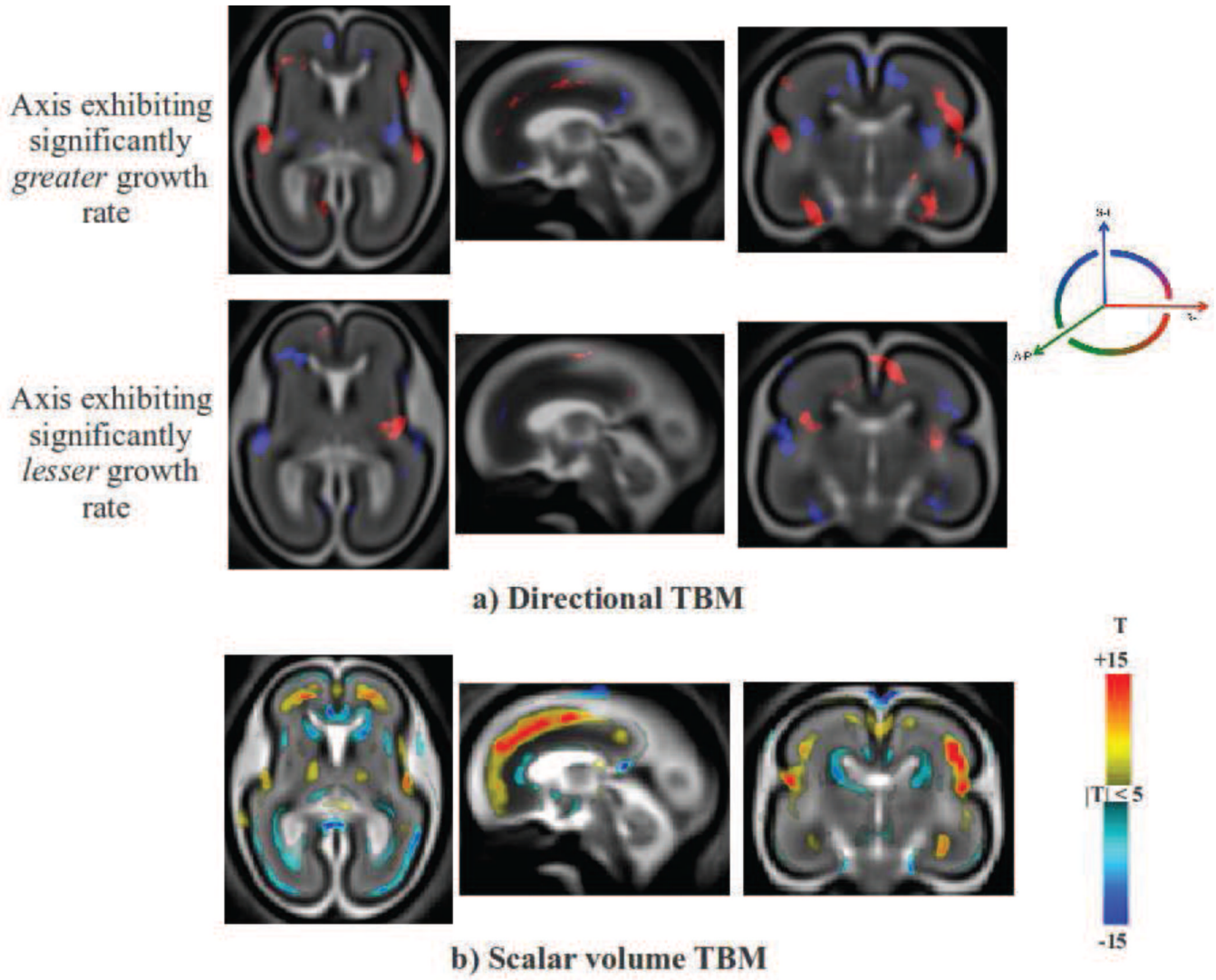

Figure 14.
Comparing directional TBM results to scalar volume TBM. a) An overview of the major changes in directional growth rate detected by the proposed method. b) Significant changes in growth rate detected using scalar volume based TBM alone. Major changes detected by both methods occur at similar locations. In addition to detecting volume changes, directional TBM allows us to localize anisotropic size changes that contribute to overall volume changes in the brain.